Advanced physico-chemical characterization of chitosan by means of TGA coupled on-line with FTIR and GCMS: Thermal degradation and water adsorption capacity

UNIVERSITÀ DEGLI STUDI DI TORINO

Advanced physico-chemical characterization of chitosan by means of TGA coupled on-line with FTIR and GCMS: Thermal degradation and water adsorption capacity

Ingrid Corazzari,[a,b,c] Roberto Nisticò,[a,b,*] Francesco Turci,[a,b,c] Maria Giulia Faga,[d] Flavia Franzoso,[a] Silvia Tabasso,[a] Giuliana Magnacca[a,b]

[a] University of Torino, Department of Chemistry, Via P. Giuria 7, 10125 Torino, Italy
[b] NIS Centre of Excellence, Via P. Giuria 7, 10125 Torino, Italy
[c] "G. Scansetti" Interdepartmental Centre for Studies on Asbestos and other Toxic Particulates, Via P. Giuria 7, 10125 Torino, Italy
[d] CNR-IMAMOTER, Strada delle Cacce 73, 10135 Torino, Italy
* Corresponding author. E-mail: roberto.nistico@unito.it, Tel. +39-011-6707533, Fax: +39-011-6707855

Abstract
In this study, chitosan, a commercially-available linear polysaccharide mainly used as antibacterial agent, functional coating and drug-delivery system, is investigated to enlighten both water interactions and its thermal stability by using a set of complementary advanced thermal techniques, rarely applied in polysaccharides characterizations. DSC and TGA, here coupled with FTIR and GCMS analysis of the exhausted gas, were used to reveal thermal events and identify degradation products as a function of the temperature: three main steps in chitosan (N-deacetylation degree, DD = 78%) thermal degradation were highlighted and mechanism proposed. In order to make a comparison with other analogous polymeric systems and validate the results obtained, a medical grade chitosan (DD > 93%) and a commercial chitin were investigated too. Moreover, the water adsorption capacity of chitosan (DD = 78%) was followed by using thermo-microgravimetry (TMG) and the distinction between weight losses of both physically and chemically adsorbed water molecules was achieved. The approach followed allows a complete characterization of the thermal behaviors of the chitosan and highlights the need for complementary advanced thermal techniques in the detailed characterization of complex biopolymers.

Keywords: Biopolymer; Chitosan; Hygroscopic property; Thermal degradation; Water loss.

1. Introduction
Chitosan is a bio-based polymer derived from the N-deacetylation of chitin, i.e. the most abundant natural amino polysaccharide, as it is a component of crabs and shrimps shells, cuticles of insects and cell walls of some fungi [1].
Both chitin and chitosan are b (1-4) glycans whose chains are formed by 2-acetamide-2-deoxy-D-glucopyranose and 2-amino-2-deoxy-D-glucopyranose units [2]. The chemical formula of this class of polymers is $(C_6H_{10}O_4N)_n$.
The N-deacetylation degree (DD in the following), which represents the molar fraction of N-deacetylated units in the polymer chain, has been largely used as a parameter for distinguishing chitin and chitosan, however a sharp nomenclature border has not been well defined. In fact, natural chitin possesses a 10% of N-deacetylated units and commercialwater-soluble chitin can have DD < 50%. Conventionally, chitin with higher values of N-deacetylation (DD = 70-90%) are usually named chitosan [3,4], thus both chitin and chitosan can be considered as random copolymers of the two units (i.e. the acetamide-containing moiety and the aminocontaining one).
Most of the applications of chitosan are based on the polyelectrolytic nature and chelating ability of the amino groups of the macromolecule. In fact, in an acidic solution, amino groups of chitosan are protonated to $-NH_3^+$, thus polyelectrolytic and chelating properties of chitosan are mainly governed by the acidity of the $-NH_3^+$ [5].
Due to its very peculiar physico-chemical and biological properties, chitosan and derivatives find applications in many fields, such as: waste water treatment for adsorption of heavy metals [6], dyes

[7] and hydrocarbons [8]; as moisturizing and conditioning product in the cosmetics industry [9]; as a protective agent against oxidation for seeds and fruits in agriculture industry [10]; as drug-delivery and antimicrobial agent in biomedical field [11-13]. Because of its antibacterial properties, chitosan is utilized for food packaging and to produce bandages and sutures since it does not cause allergic reactions [14,15]. Finally, chitosan-based membranes are used in the water softening processes [16].

Since carbohydrates can be used as cheap precursors for the carbons synthesis and considering the growing interest in the development of advanced materials for energy applications [17], in particular for the production of mesoporous and N-doped carbons and coals for catalysis and ion storage batteries, it goes without saying that chitosan (with its precious amino groups) can be considered one of the most promising precursor of N-doped carbon source [18-20].

In view of the wide number of applications involving chitosan, several studies examined both its physico-chemical properties and chemical structures [7,21-23].

Many authors [24e26] investigated the kinetic aspects related to the thermal degradation of chitosan and its derivates by using thermogravimetric analyses (TGA), both in air or in nitrogen atmosphere. In some cases, differential scanning calorimetry (DSC) tests were conducted in order to highlight phase transitions in water/chitosan systems [27] or clarify each single-step of the thermal degradation mechanism [28].

Currently, it appears clear as the chemistry of chitosan is closely linked to the availability of polar groups present in the polymer structure (amino and hydroxyl moieties) and to the interactions that these species can establish with water molecules. In particular, it is well known that the amino groups of chitosan chains can be involved in chelation processes (such as the formation of chitosan-metal ions complexes), which affect the conformation of the polymer and consequently its thermal stability [29].

An interesting study describing an adsorption isotherm of water vapor on chitosan characterized by different molecular weights (i.e. viscosities) were presented in Ref. [30]. The authors considered different adsorption sites, i.e. hydroxyl groups, amino groups (whose amount increases with the molecular weight of chitosan) and polymer chain ends (essentially hydroxyl or aldehyde groups, whose concentration increases decreasing the molecular weight of chitosan). The hydration enthalpies related to -OH and -NH_2 groups are very different (23.9 and 70.3 kJ mol^{-1}), therefore they are theoretically distinguishable. Unfortunately, the variability of the effects given by the not-measurable chitosan chains length and crystallinity does not allow to distinguish the single contributions and the only conclusion obtained is phenomenologic, i.e. increasing the chitosan molecular weight the adsorbed amount of water slightly decreases and the energy parameter (taking into account the interaction of water molecules with the functional groups present in chitosan) decreases.

Other attempts to determine chitosan features were made using dynamical mechanical thermo analysis (DMTA) that allowed to assess the role of plasticizer to water present in small amount between the “dry” chitosan chains [31].

Although the number of investigations performed on chitosan, little is known about its thermal behaviors, which rises particular interest for its possible role in the synthesis of doped carbon-based material.

The characterization is complicated by many problems, among them the extremely large number of materials named chitosan (different DD and molecular weight confer different properties to the polymer), and the presence of a large amount of water interacting with the carbohydrate and affecting the chitosan molecules organization, which for instance, renders chitosan Tg determination difficult to measure [32-35].

Aim of this work is to clarify both the water effect on the partially N-deacetylated chitosan (DD = 78%) structure and the thermal stability and degradation mechanism of this class of biomacromolecules using some physico-chemical techniques, specifically electron microscopy (SEM-EDS), spectroscopy (NMR, FTIR) X-ray diffraction (XRD), gas-volumetric N_2

adsorption/desorption experiments and thermal analyses (DSC, TGA, TGA-FTIR-GCMS, thermo-microgravimetry with water vapor adsorption). Since this partially N-deacetylated chitosan is the most commercially used form, it required a more detailed physico-chemical characterization.
Moreover, for the sake of comparison, other polymeric systems belonging to this class, namely a medical grade chitosan (DD > 93%) and a commercial chitin, were investigated by means of TGA-FTIR measurements.
Among all the techniques here selected, TGA-FTIR-GCMS confirms to be a very useful tool since it was already successfully employed to unveil the amount and the nature of chemical moieties evolved from different complex composite materials [36-38], as well as the DD.

2. Experimental

2.1 Materials and physic-chemical characterization

Partially N-deacetylated chitosan (DD = 75-85%) of medium molecular weight (Mv = 190-310 kDa) with Brookfield viscosity of 200-800 cps (from crab shells, Aldrich, CAS 9012-76-4) has been fully characterized, whereas medical grade chitosan (DD > 93%) with Brookfield viscosity of 350-750 cps (Heppe Medical Chitosan GmbH, CAS 9012-76-4) and commercial chitin (from snow crab, Heppe Medical Chitosan GmbH, CAS 1398-61-4) were thermally investigated for the sake of comparison. All chemicals were used without further purifications, in order to keep unaltered the sample properties, which could be modified by drying and/or thermal treatments
Scanning Electron Microscopy (SEM) analyses were carried out using a ZEISS EVO 50 XVP with LaB_6 source, equipped with detectors for secondary electrons collection and EDS probe for elemental analyses. Since the analyzed sample is insulating, chitosan was covered with a gold layer of ca. 15 nm of thickness before the analysis to avoid any charging effect (Bal-tec SCD050 sputter coater). Therefore, the presence of gold in EDS spectra (principal signal at 2.2 keV) is due to this step and will not be evidenced in the following data discussion.
X-Ray Diffraction (XRD) patterns were obtained using the diffractometer PW3040/60 X'Pert PRO MPD from PANalytical, in Bragg-Brentano geometry, equipped with the high power ceramic tube PW3373/10 LFF source with Cu anode.
FTIR spectra were recorded in both transmission and Attenuated Total Reflection mode (diamond cell for single reflection) in a Bruker IFS28 spectrophotometer equipped with Globar source, DTGS detector, and working with 128 scans at 4 cm^{-1} of resolution in the range 4000e400 cm^{-1}. FTIR analysis in transmission mode was carried out using the sample dispersed in KBr (1:20 weight ratio). ATR spectra were obtained directly on the powdery sample repeating the acquisition for three times.
N_2 adsorption-desorption experiments were carried out by means of ASAP 2020 instrument (Micromeritics) in order to determine the specific surface area (BET model) [39] and porosity (DFT model) of the sample. The density functional theory (DFT) was applied in order to consider simultaneously micro and mesoporosity [40,41]. Powdery sample (ca. 1 g) was outgassed for about 48 h at Room Temperature (RT) in vacuum (residual pressure 10^{-2} mbar) to ensure complete removal of atmospheric contaminants from the surface before analysis.

2.2 Determination of the N-deacetylation degree (DD) by 1H NMR spectroscopy

The NMR experiments were performed with a Bruker Avance 200 NMR spectrometer at RT; the ^1H chemical shifts are reported relative to residual solvent signals (D_2O).
For 1H NMR measurements, a solution of 2 wt.% of chitosan (DD = 78%) powder in D_2O/CD_3COOD 2 vol.% was prepared and mixed by magnetic stirring overnight at RT. As reported in literature [42], the N-deacetylation degree (DD) is calculated by using the following Equation (1).

$$DD(\%) = [1-((1/3*I_{CH3})/(1/6*I_{H2-H6}))]$$

where I_{CH3} is the integral intensity of the -CH_3 residue of N-acetyl groups and I_{H2-H6} is the sum of the integral intensity of the protons H2, H3, H4, H5, H6 and H6'.

2.3 DSC measurements and calorimetric characterization

Differential Scanning Calorimetry (DSC) studies were carried out using TA instruments temperature modulated DSC (TA Q200). Dry nitrogen gas was purged into the DSC cell with a flow rate of 50 mL min^{-1}. The sample mass was kept at about 10 mg in an aluminum hermetic pan. The phase transition peak area compared with the calorimetric constant determined for an appropriate standard material allows obtaining the phase transition enthalpy. The experimental thermal programs used for sample treatments are the following:

- First program (20 °C/min-190-RT-190): a ramp of 20 °C min^{-1} starting from 40 °C up to 190 °C for the heating cycle, a ramp of 10 °C min^{-1} down to RT for the cooling cycle, then a second heating cycle.
- Second program (2 °C/min-400): a ramp of 2 °C min^{-1} starting from 40 °C up to 400 °C.
- Third program (10 °C/min-400): a ramp of 10 °C min-1 starting from 40 °C up to 400 °C.

The successive repetition of the same heating cycle allows evidencing the presence of some irreversible phenomena.

2.4. Thermo(micro)gravimetric study and water loss determination

To assess the nature and the amount of the species evolved during the thermal analysis, an ultra-microbalance (sensitivity 0.1 µg) connected with a time-resolved FTIR and GCMS detectors was employed. The powders (ca. 10 mg) were placed in an open platinum pan and heated from 30 to 800 °C at the rate of 10 °C min^{-1} under dynamic nitrogen atmosphere (gas purity: 99.9995%; flow rate: 35 mL min^{-1}) in a Pyris 1 TGA from Perkin-Elmer (Waltham, MA, USA). The gas evolved during the heating ramp was piped (gas flow 65 mL min^{-1}) via pressurized heated transfer line (Redshift S.r.l. - Vicenza, Italy) and analyzed continuously by the FTIR (Spectrum 100, Perkin-Elmer), equipped with a thermostated conventional gas cell. Temperature/time-resolved spectra were acquired in the 4000-600 cm^{-1} wavenumber range with a resolution of 0.4 cm^{-1} and analyzed with the Spectrum software (Perkin-Elmer). Temperature-resolved infrared profiles of each single moiety desorbed from samples were obtained from the intensity of a representative peak of the investigated species.

At a given temperature/time, the evolved gas was automatically collected (ca. 100 µL) and injected into a Clarus 500S gas chromatograph (Perkin-Elmer) equipped with a standard non-polar fused silica capillary column Elite 5MS (Perkin-Elmer). The substances eluted were identified with an integrated Clarus 560S mass spectrometer (Perkin-Elmer) as detector. Total Ion Count (TIC) chromatograms were reported as well as some detailed mass spectra of specific chromatographic peaks. Analyses of the average mass spectra calculated at the chromatographic peak middle height were carried out with NIST MS Search Software.

Thermo-microgravimetry (TMG) studies were performed with a microbalance apparatus (IGA002 from Hiden Isochema Ltd., Warrington, UK). The microbalance controller of the instrument has sensitivity with an intrinsic accuracy equivalent to 0.006 wt.% of the selected weighing range (ca. 100 mg) [43]. For all measurements, chitosan powder was transferred into the microbalance inside a steel reactor that allows thermal treatments up to 500 °C, either in vacuum or in a controlled atmosphere. The programs used for sample treatments were the following:

- First program: outgassing at RT.
- Second program (3 °C/min-130-RT): a ramp of 3 °C min^{-1} up to 130 °C for the heating cycle and then a ramp of 3 °C min^{-1} down to RT for the cooling cycle.

Water vapor adsorption was tested in order to verify the reversibility of the thermal-induced water weight loss. Therefore, admissions of 20 mbar of water vapor (admission rate 1 mbar min^{-1}), was performed on dehydrated samples (after thermal program 3 °C/min-130-RT) and the removal examined, upon thermal programs described above. RT corresponds to the temperature of 25 ± 2

°C. All the treatments (outgassing, heating/cooling and water vapor adsorption) were carried out until sample weight equilibrium was reached.
Moreover, a further measurement without samples inside the apparatus was done, in order to evaluate the adsorption capacity of instrument configuration. Negligible variations are obtained compared to the amounts examined, therefore no corrections were made.

3. Results and discussion

3.1 Morphological characterization of the partially N-deacetylated chitosan and determination of the DD

SEM image of partially N-deacetylated commercial chitosan powder is reported in Fig. 1 both at low (A) and high (B) magnifications. The powder presented oval pleated shaped particles with a diameter size of about 200 mm. EDS analysis (not reported for sake of brevity) confirmed the presence of C, N and O contributions.
Chitosan powder was characterized also by XRD, in order to verify the biopolymer crystallinity. In Fig. ESI-1 (reported in the Electronic Supporting Information, ESI in the following) two broad reflections, typical of mainly amorphous structures with a short-range order, are visible. Both contributions are attributable to α-chitin moieties (chitosan precursor), the first one at $2\theta = 9.3°$ due to (020) plane, narrower because associated to the most ordered moieties involving the acetamide groups [44,45], the second one at $2\theta = 19.9°$ due to the (110) plane of α-chitin, wider because affected by the amorphous structure of chitosan. These signals confirmed that chitin units were still present in chitosan framework generating a statistic copolymer.
The presence of N-acetylated units was also confirmed by using ^{1}H NMR technique. The spectrum obtained is shown in Fig. 2 and typical signals of chitosan structural hydrogen atoms were registered [24,42]. In particular, signals between 3.4 and 4.0 ppm correspond to the hydrogen atoms bonded to the carbon atoms 3, 4, 5 and 6 of the glucopyranose unit. A distinct signal centered at 3.18 ppm corresponds to the hydrogen atom bonded to the carbon atom 2 of the glucopyranose unit, whereas the signal centered at 1.99 ppm corresponds to the hydrogen atoms of acetamido methyl-groups. This spectrum and Equation (1) allowed to determine the average DD of 78% [42].
The study of specific surface area and porosity of such material was achieved using gas-volumetric adsorption/desorption of N_2 at 77 K. Only indicative values relative to the specific surface area and porosity of the material were achieved, because of the very low extent of N_2 adsorption shown by chitosan (DD = 78%). For this reason the isotherms are not shown but the main results are discussed. The BET surface area, obtained after a prolonged outgassing of the chitosan powder at RT with the aim of removing the large amount of physisorbed water without modifying the structure of the sample, corresponds to ca. 2 $m^2\ g^{-1}$. The isotherm is of the III type, with a thin hysteresis loop of H3 type (from IUPAC classification) in the relative pressure range 0.7-1: this should indicate that a small amount of pores are present and given by non-rigid aggregates of plate-like particles (as confirmed by SEM micrographs reported in Fig. 1).

3.2 Thermal degradation of chitosan

DSC curves of chitosan (DD = 78%) are obtained at different heating rates in nitrogen flow (thermal program 10 °C/min-400 and 2 °C/min-400). Two well defined signals (due to thermal transitions) are visible in the curve obtained at heating rate of 10 °C/min.
The first signal (T < 100 °C, endothermic) is commonly associated to the evaporation of physisorbed water, whereas the second one (occurring at ca. 300 °C, exothermic) should be related to the decomposition of chitosan (Fig. 3(A)). As shown in Fig. 3(B), the decrease of heating rate from 10 to 2 °C/min allows evidencing that the degradation of chitosan begins at temperature lower than 250 °C through a complex pathway evidenced by the shoulder present at higher temperatures. The thermal event due to glass transition of the polymer was not evidenced, even in a run performed at high heating rate to give evidence of modest thermal events (see Fig. ESI-2).

Chitosan (DD = 78%) thermal behaviour was also analyzed by TGA in the temperature range from 30 to 800 °C under dynamic N_2 atmosphere. The volatile species evolved during the heating ramp were continuously monitored by the FTIR detector. The FTIR profiles of the volatiles evolved, expressed as ppm/mg of sample, were determined relating the IR absorbance at a specific wavenumber (namely 3566 cm^{-1} for H_2O, 965 cm^{-1} for NH_3, 2185 cm^{-1} for CO, 2359 cm^{-1} for CO_2, 1179 cm^{-1} for acetic acid and 3016 cm^{-1} for CH_4) to concentration according to the Lambert-Beer's law relationship employing the spectra of each species at known concentration from the instrumentation database. In Fig. 4, the weight loss % and its derivative curve (upper panel) are compared to the FTIR profiles (lower panel) obtained for each gaseous species identified in the evolved gas (representative FTIR spectra are reported in Fig. ESI-3).

Chitosan (DD = 78%) exhibited an overall weight loss of about 67 wt.%. In the temperature range between 30 and 150 °C a single process, evidenced by a broad minimum peak on the derivative curve (highest rate at 76 °C), took place causing a first weight loss of ca. 5 wt.%. FTIR analysis identified unambiguously this weight loss with water desorption. No other volatiles (e.g. organic contaminants with low boiling point) were present in the gas evolved in this temperature range. The FTIR results confirmed what reported in previous thermal studies on chitosan, where such weight loss was commonly assigned to water desorption [27,28]. The temperature of this process indicated that such water was loosely bound, i.e. physisorbed, at the chitosan surface.

The material weight remained stable up to ca. 250 °C. After this temperature a dramatic weight loss process took place with the highest rate at 334 °C. At 350 °C a change of the thermogram curve slope suggests that a second process, slower than the previous one, took place. The correspondent derivative curve exhibited a long tail which reached the zero value at ca. 750 °C with no evident distinct events. The FTIR analysis of the evolved gas evidenced that a complex gaseous mixture mainly composed by H_2O, NH_3, CO, CO_2, CH_3COOH and CH_4 (representative spectra are reported in Fig. ESI-3) was released during the degradation of chitosan. Monitoring the evolution of such species in temperature/time scale, the FTIR analysis unveiled a complex degradation pattern characterized by steps partially overlapped. A main process involving the release of H_2O, NH_3, CO, CO_2 and CH_3COOH was observed in the temperature range 250-450 °C and caused a weight loss of 54 wt.%. This process was assigned to the pyrolytic degradation of chitosan, as well assessed in the literature [25]. The release of NH_3 started at a lower temperature than the other species (it reaches its highest rate at 325 °C) suggesting that the NH_3 formation requires a low activation energy. Afterwards, a second process characterized by the release of CH_4 took place in the range 450-750 °C (highest rate at ca. 590 °C) and caused a modest weight loss (9 wt.%). This step suggests that a further modification of the material occurs when the structure is almost completely reduced causing the production of methane and the consequent formation of a graphite-like structure via dehydrogenation mechanism, as suggested in the literature [24,46].

For the sake of comparison, two other systems belonging to this class of biopolymers, namely a medical grade chitosan (DD > 93%) and a commercial chitin, were investigated by means of TGA-FTIR measurements (see Figs. ESI-4 and ESI-5, respectively). As expected, the thermal behavior of medical grade chitosan (DD > 93%) was similar to that registered for chitosan (DD = 78%), even if the weight loss observed was slightly lower (51 wt.%). Analogously, FTIR analysis evidenced that the acetic acid amount for medical grade chitosan was lower than that measured for chitosan (DD = 78%) as expected considering the DD of the two biopolymers. Vice versa, the thermal degradation of chitin exhibited a different behavior and a significant shift of the main process (i.e. pyrolysis, highest rate at ca. 430 °C) towards higher temperatures was observed. Moreover, the FTIR analysis evidenced a single-step degradation pattern characterized by the release of H_2O, CO, CO_2 and CH_3COOH in the temperature range 280-500 °C causing a weight loss of ca. 80 wt.%. Conversely, respect to the two chitosan samples, NH_3 release was not observed. As reported in the experimental section, the gases evolved from TGA are collected in continuous into a cell and the gas concentration (expressed in ppm/mg of sample) was calculated from the FTIR intensity according to the Lambert-Beer's law. Combining the FTIR data with the TGA quantitative determinations, the

weight loss due to each evolved species was estimated. The total amount of each species formed during the pyrolysis was quantified by the following procedure:

i. Integrating the FTIR profile in the temperature range 250-450 °C.
ii. Calculating the ratio of each gaseous product with respect to all the species evolved.
iii. Normalizing the weight loss due to pyrolysis to each gaseous product ratio.

The results obtained are reported in Table 1.

Since acetic acid amount released is correlated to the DD, we focused on the analysis of this species. The weight loss due to acetic acid is 28.7 wt.% for chitin, 13.8 wt.% for chitosan (DD = 78%) and 4.30 wt.% for medical grade chitosan (DD > 93%). The amount of acetylated units, complimentary to DD value, in chitosan (DD = 78%), previously determined by ^{1}H NMR (Fig. 2), is 22%. This amount corresponds to 13.8 wt.% in TGA curve. Proportionally the acetylated units calculated for chitin (weight loss 28.7 wt.%) is 46% and 9% for medical grade chitosan (DD > 93%, weight loss 4.30 wt.%). Furthermore, kinetics information can be gained by monitoring the amount of species evolved as a function of temperature/time. In fact, in principle, integrating the FTIR curves in the temperature range relative to the species release and normalizing them to the weight loss% assessed by TGA, a quantitative determination of the degradation products as a function of the temperature/time can be achieved. The summary of the entire calculation procedure is reported in Fig. ESI-6 relatively to the acetic acid release profile for chitosan (DD = 78%). Fig. 5 shows the N-deacetylation kinetics (i.e. acetic acid release) as a function of temperature/time for the three biopolymers studied. Both chitosan samples (curves b and c) exhibited the highest rate of N-deacetylation at ca. 350 °C and chitin (curve a) at ca. 440 °C.

To further unveil secondary products of chitosan degradation, the gas evolved during the chitosan (DD = 78%) pyrolysis was also analyzed by GCMS sampling the gas evolved from the TGA at 334 °C. The gas chromatogram (Fig. ESI-7) evidenced the presence of several species identified by acetic acid methyl ester (A) and the acetohydroxamic acid (D), together with several N- and O-heterocyclic molecules including pyrazine (B), pyridine and pyrrole superimposed (C), 2-(5H)-furanone (E), 2-methylpyridine (F), methylpyrazine (G), 3-methyl-(1H)-pyrrole (H), ethylpyrazine (I), and acetylpyrazine (J). Mass spectra obtained for each peak are reported in the ESI (Fig. ESI-8). Pyrazines, the most important products in the pyrolysis of chitosan, have already been detected together with other heteroaromatic compounds such as pyridines, pyrroles and furans [47]. After the N-deacetylation of glucosamine, as evidenced by the loss of acetic acid, the reaction of a-amino carbonyls produces pyrazines and pyridines, through the formation of imine intermediates. On the other hand, furan rings derive from the dehydration of polyhydroxypyrazines, dimerization products of glucosamine [48]. Both processes involve the elimination of water, whereas ammonia is released as a consequence of furans formation.

The results above described indicate that the amino groups on the glucosamine structure can be released in two different ways: via ammonia release (as highlighted by FTIR analysis) and via heteroaromatic rings formation (as highlighted by GCMS) confirming that the degradation of the biopolymer can take place by random breaking of C-O-C skeletal bonds as suggested in the literature [12,43]. The proposed reactivity is supported by the exothermic peak evidenced by the DSC analysis (Fig. 3), whereas desorption would have been evidenced by an endothermic peak.

The infrared spectroscopic characterization of chitosan (DD = 78%) sample after different thermal treatments is reported in Fig. 6. All the presented FTIR spectra were collected in transmission mode.

The FTIR spectrum of chitosan before thermal treatment (curve A) shows the classic peaks assigned to polysaccharide structures. The main signals in the spectrum are: a strong and broad band due to the axial O-H and N-H stretching centered at 3440 cm^{-1}, C-H stretching bands registered at 2870-2880 cm^{-1}, the absorption centered at 1655 cm^{-1} attributable to the axial C=O stretching of the acetamido groups (named amide I), the one at 1580 cm^{-1} attributable to the angular deformation of N-H bonds of the amino groups, the bands at 1420-1477 cm^{-1} resulting from the coupling of C-N axial stretching and N-H angular deformation, the sharp band at 1377 cm^{-1} assigned to the CH_3

symmetrical deformation mode [24,28]. Finally, finger print bands, extremely useful for evidencing chitosan presence even in low amounts (for instance for chitosan coatings deposition [11,12]), are due to skeletal signals (vibrations of glycosidic bonds, C-O and C-O-C stretching) absorbing between 1150 cm^{-1} and 900 cm^{-1}.
No modifications were evidenced by the spectrum of the sample thermally treated at 200 °C in nitrogen flow (curve B), whereas the complete sample degradation was confirmed by the latter spectrum (curve C), related to the sample after treatment at 800 °C in nitrogen flow. It can be assumed that the material treated at 800 °C losses all the functional groups originally present (amino and hydroxyl groups), and also its polysaccharide skeleton is completely denatured, leaving a graphite-like structure whose typical IR feature is visible at around 1600 cm^{-1}.

3.3. Interacting water determination

As previously reported in literature, water can interact with chitosan macromolecules in three different physical states: as physically adsorbed water (i.e. weakly interacting), as chemically adsorbed water (i.e. strongly interacting), and as plasticizer when present between dried polymer chains [30].
Since the latter is difficult to be observed in powdery samples (its presence becomes relevant in hydrogels, for instance), we focused our attention on the two main adsorption states, physically and chemically interacting water molecules, in order to provide some quantitative information concerning the two contributions.
Thermo-microgravimetric analyses were carried out to discriminate and quantify water desorption in terms of outgas-induced and thermally-induced chitosan weight losses (physisorbed and chemisorbed water, respectively).Water vapor uptakes were subsequently carried out to verify chitosan water adsorption capacity and, finally, the reversibility of chitosan hydration/dehydration phenomena was evaluated.
In order to have a clean starting material, chitosan (DD = 78%) powders were firstly subjected to different dehydration treatments: in particular physisorbed water was desorbed by outgassing at RT whereas chemisorbed water was removed by using a thermal program (3 °C/min-130-RT). Compared to the starting sample weight (reported as 100 wt.%), chitosan weight becomes 92.60 wt.% after the first outgassing at RT and 92.27 wt.% after the second thermal treatment, allowing to assign the weight loss of 7.40 wt.% to the physically interacting water and that of 0.33 wt.% to the chemically interacting water, for a total weight loss of 7.73 wt.%.
Fig. 7 reports the weight changes experimented by chitosan (DD = 78%) thermally treated at 130 °C, cooled down at RT, and submitted to hydration upon admission of 20 mbar of water vapor, i.e. with the microbalance chamber saturated with water. This experiment should allow quantifying the water adsorption capacity of chitosan under study. In all cases the weight values do not show significant trend over time, indicating that no relevant modification of the sample occurred. Moreover, the reversibility of adsorption/desorption phenomena were confirmed, thus the average values of three cycles of chitosan hydration/dehydration are presented.
An average weight increase of 15.98 wt.% ±0.62 is observed for sample dehydrated and contacted with water vapor. Relatively to this amount, the outgassing at RT allows to quantify the physically interacting water amount which corresponds to 15.84 wt.% ±0.72, since the chemisorbed water residue calculated is 0.14 wt.% ±0.10.
The physisorbed water value is much higher than that of the original chitosan (DD = 78%) sample (7.40 wt.%), thus this is an indication that the amount of water physisorbed by chitosan (as it is) is very low in comparison to the amount captured when dehydrated chitosan is exposed to pure water vapor.
Concluding, it is possible to assume that water vapor adsorbed by dried chitosan powder is almost completely in the form of physisorbed molecules and to confirm the important water adsorption capacity of dried chitosan.

4. Conclusions

In this study, a partially N-deacetylated chitosan powder, previously characterized in terms of physico-chemical features and N-deacetylation degree (DD = 78%), was investigated to enlighten both water interaction and thermal properties.

The water weight loss was quantified by thermo-microgravimetric analyses and a distinction between adsorbed water molecules (mostly physically adsorbed) was achieved.

The coupled use of DSC and TGA equipped with FTIR-GCMS devices allowed to determine chitosan dehydration and decomposition processes. Three main degradation steps were evidenced, each single degradation product was recognized, and the mechanism of thermal decomposition proposed. In particular, nitrogen-containing species were released in two different forms: inorganic volatile product as ammonia and organic ones as heteroaromatic species. The formation of these heteroaromatic species, together with the presence of graphite-like residues after treatment at high temperature in inert atmosphere, suggests a potential application of chitosan as precursor in the production of N-doped carbon-based materials, pointing out the best conditions needed (i.e. temperature and heating rate).

Moreover, the thermal degradation of medical grade chitosan (DD > 93%) and commercial chitin was also analyzed by means of TGA-FTIR and compared with chitosan (DD = 78%) for validating the results obtained. Differences were highlighted and thoroughly discussed. In particular, the amount of each degradation product as a function of the temperature/time was monitored and a correlation between the total weight loss due to acetic acid formation and the N-deacetylation degree (DD)was evidenced. All the results here discussed confirmed the usefulness of TGA-FTIR-GCMS technique for the resolution of complex degradation patterns of polymers and biopolymers.

5. Acknowledgements

The authors would like to thank Dr. D. Scalarone and Dr. D. Lussana for their suggestions and comments. The TGA-FTIR-GCMS measures have been obtained with the equipment acquired by the “G. Scansetti” Interdepartmental Center for Studies on Asbestos and Other Toxic Particulates thanks to a grant by the Compagnia di San Paolo, Torino, Italy..

References

[1] Muzzarelli RAA. Chitin. Oxford: Pergamon Press Ltd; 1977.

[2] Signini R, Campana-Filho SP. On the preparation and characterization of chitosan hydrochloride. Polym Bull 1999;42:159-166.

[3] Pillai CKS, Paul W, Sharma CP. Chitin and chitosan polymers: chemistry, solubility and fiber formation. Prog Polym Sci 2009;34:641-678.

[4] Knaul JZ, Hudson SM, Creber KAM. Crosslinking of chitosan fibers with dialdehydes: proposal of a new reaction mechanism. J Polym Sci B Polym Phys 1999;37:1079-1094.

[5] Park SY, Marsh KS, Rhim JW. Characteristics of different molecular weight chitosan films affected by the type of organic solvents. J Food Sci 2002;67:194-197.

[6] Vijaya Y, Popuri SR, Boddu VM, Krishnaiah A. Modified chitosan and calcium alginate biopolymer sorbents for removal of nickel (II) through adsorption. Carbohydr Polym 2008;72:261-271.

[7] Wan Ngah WS, Teong LC, Hanafiah MAKM. Adsorption of dyes and heavy metal ions by chitosan composites: a review. Carbohydr Polym 2011;83:1446-1456.

[8] Babel S, Kurniawan TA. Low-cost adsorbents for heavy metals uptake from contaminated water: a review. J Hazard Mater 2003;97:219-243.

[9] Rinaudo M. Chitin and chitosan: properties and applications. Prog Polym Sci 2006;31:603-632.

[10] Falcon AB, Cabrera JC, Costales D, Ramírez MA, Cabrera G, Toledo V, et al. The effect of size and acetylation degree of chitosan derivatives on tobacco plant protection against phytophthora parasitica nicotianae. World J Microbiol Biotechnol 2008;24:103-112.

[11] Nisticò R, Faga MG, Gautier G, Magnacca G, D'Angelo D, Ciancio E, et al. Physico-chemical characterization of functionalized polypropylenic fibers for prosthetic applications. Appl Surf Sci 2012;258:7889-7896.
[12] Avetta P, Nisticò R, Faga MG, D'Angelo D, Aimo Boot E, Lamberti R, et al. Hernia-repair prosthetic devices functionalised with chitosan and ciprofloxacin coating: controlled release and antibacterial activity. J Mater Chem B 2014;2:5287-5294.
[13] Sanyakamdhorn S, Agudelo D, Tajmir-Riahi HA. Encapsulation of antitumor drug doxorubicin and its analogue by chitosan nanoparticles. Biomacromolecules 2013;14:557-563.
[14] Rabea EI, Badawy MET, Stevens CV, Smagghe G, Steurbaut W. Chitosan as antimicrobial agent: applications and mode of action. Biomacromolecules 2003;4:1457-1465.
[15] Raafat D, von Bargen K, Haas A, Sahl HG. Insights into the mode of action of chitosan as an antibacterial compound. Appl Environ Microbiol 2008;74:37643773.
[16] Ladet S, David L, Domard A. Multi-membrane hydrogel. Nature 2008;452:76-79.
[17] Li XH, Antonietti M. Metal nanoparticles at mesoporous N-doped carbons and carbon nitrides: functional Mott-Schottky heterojunctions for catalysis. Chem Soc Rev 2013;42:6593-6604.
[18] Wang Z, Qie L, Yuan L, Zhang W, Hu X, Huang Y. Functionalized N-doped interconnected carbon nanofibers as an anode material for sodium-ion storage with excellent performance. Carbon 2013;55:328-334.
[19] Antonietti M, Titirici MM. Coal from carbohydrates: the “chimie douce” of carbon. Comptes Rendus Chim 2010;13:167-173.
[20] Fechler N, Wohlgemuth SA, Jaker P, Antonietti M. Salt and sugar: direct synthesis of high surface area carbon materials at low temperatures via hydrothermal carbonization of glucose under hypersaline conditions. J Mater Chem A 2013;1:9418-9421.
[21] Muzzarelli RAA. Chitins and chitosans for the repair of wounded skin, nerve, cartilage and bone. Carbohydr Polym 2009;76:167-182.
[22] Muzzarelli RAA, Boudrant J, Meyer D, Manno N, DeMarchis M, Paoletti MG. Current views on fungal chitin/chitosan, human chitinases, food preservation, glucans, pectins and inulin: a tribute to Henri Braconnot, precursor of the carbohydrate polymers science, on the chitin bicentennial. Carbohydr Polym 2012;87:995-1012.
[23] Muzzarelli RAA. Chitosan composites with inorganics, morphogenetic proteins and stem cells, for bone regeneration. Carbohydr Polym 2011;83:1433-1445.
[24] de Britto D, Campana-Filho SP. A kinetic study on the thermal degradation of N, N,N-trimethylchitosan. Polym Degrad Stab 2004;84:353-361.
[25] de Britto D, Campana-Filho SP. Kinetics of the thermal degradation of chitosan. Thermochim Acta 2007;465:73-82.
[26] Pawlak A, Mucha M. Thermogravimetric and FTIR studies of chitosan blends. Thermochim Acta 2013;396:153-166.
[27] Ratto JA, Hatakeyama T, Blumstein RB. Differential scanning calorimetry investigation of phase transition in water/chitosan systems. Polymer 1995;36:2915-2919.
[28] Qu X, Wirsen A, Albertsson AC. Effect of lactic/glycolic acid side chains on the thermal degradation kinetics of chitosan derivates. Polymer 2000;41:4841-4847.
[29] Sreenivasan K. Thermal stability studies of some chitosan-metal ion complexes using differential scanning calorimetry. Polym Degrad Stab 1996;52:85-87.
[30] Gocho H, Shimizu H, Tanioka A, Chou TJ, Nakajima T. Effect of the polymer chain end on sorption isotherm of water by chitosan. Carbohydr Polym 2000;41:87-90.
[31] Khalid MN, Agnely F, Yagoubi N, Grossiord JL, Couarraze G. Water state characterization, swelling behavior, thermal and mechanical properties of chitosan based networks. Eur J Pharm Sci 2002;15:425-432.
[32] Dong Y, Ruan Y, Wang H, Zhao Y, Bi D. Studies on glass transition temperature of chitosan with four techniques. J Appl Polym Sci 2004;93:1553-1558.

[33] Ogura K, Kanamoto T, Itoh M, Miyashiro H, Tanaka K. Dynamic mechanical behavior of chitin and chitosan. Polym Bull 1980;2:301-304.
[34] Ahn JS, Choi HK, Cho CS. A novel mucoadhesive polymer prepared by template polymerization of acrylic acid in the presence of chitosan. Biomaterials 2001;22:923-928.
[35] Pizzoli M, Ceccorulli G, Sandola M. Molecular motions of chitosan in the solid state. Carbohydr Res 1991;222:205-213.
[36] Giustetto R, Wahyudi O, Corazzari I, Turci F. Chemical stability and dehydration behavior of a sepiolite/indigo Maya Blue pigment. Appl Clay Sci 2011;52:41-50.
[37] Corazzari I, Livraghi S, Ferrero S, Giamello E, Fubini B, Fenoglio I. Inactivation of TiO_2 nano-powders for the preparation of photo-stable sunscreens via carbon-based surface modification. J Mater Chem 2012;22:19105-19112.
[38] Livraghi S, Pelaez M, Biedrzycki J, Corazzari I, Giamello E, Dionysiou DD. Influence of the chemical synthesis on the physicochemical properties of N-TiO_2 nanoparticles. Catal Today 2013;209:54-59.
[39] Brunauer S, Emmett PH, Teller E. Adsorption of gases in multimolecular layers. J Am Chem Soc 1938;60:309-319.
[40] Nisticò R, Scalarone D, Magnacca G. Preparation and physico-chemical characterization of large-mesopore silica thin films templated by block copolymers for membrane technology. Microporous Mesoporous Mater 2014;190:208-214.
[41] Ou DL, Chevalier PD, Mackinnon IA, Eguchi K, Boisvert R, Su K. Preparation of microporous ORMOSILs by thermal degradation of organically modified siloxane resin. J Sol Gel Sci Technol 2003;26:407-412.
[42] Hirai A, Odani H, Nakajima A. Determination of the degree of deacetylation of chitosan by ^1H NMR spectroscopy. Polym Bull 1991;26:87-94.
[43] Hilding J, Grulke EA, Sinnott SB, Qian D, Andrews R, Jagtoyen M. Sorption of butane on carbon multiwall nanotubes at room temperature. Langmuir 2001;17:7540-7544.
[44] Jang MK, Kong BG, Jeong YI, Lee CH, Nah JW. Physicochemical characterization of alpha-chitin, beta-chitin and gamma-chitin separated from natural resources. J Polym Sci Part A Polym Chem 2004;42:3423-3432.
[45] Saito Y, Kumagai H, Wada M, Kuga S. Thermally reversible hydration of β-chitin. Biomacromolecules 2002;3:407-410.
[46] Zeng L, Qin C, Wang L, Li W. Volatile compounds formed from the pyrolysis of chitosan. Carbohydr Polym 2011;83:1553-1557.
[47] Wanjun T, Cunxin W, Donghua C. Kinetic studies on the pyrolysis of chitin and chitosan. Polym Degrad Stab 2005;87:389-394.
[48] Chen J, Ho CT. Volatile compounds formed from thermal degradation of glucosamine in a dry system. J Agric Food Chem 1998;46:1971-1974.

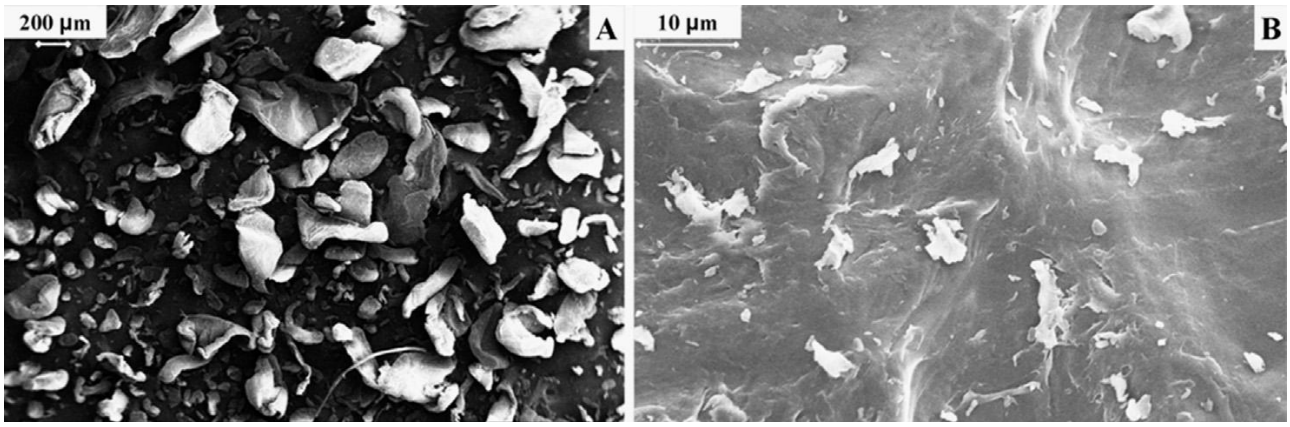

Fig. 1. SEM micrographs of partially N-deacetylated chitosan powder collected at low (A) and high (B) magnification.

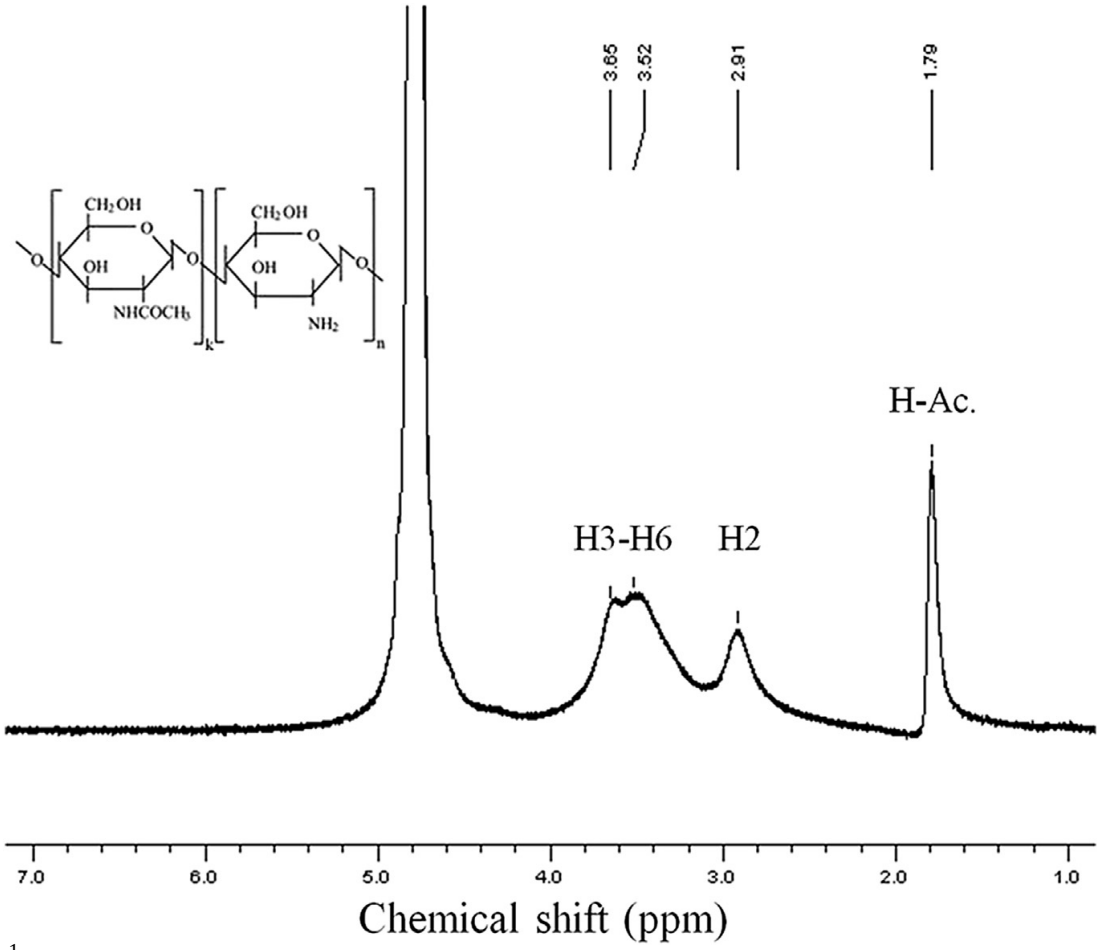

Fig. 2. ^{1}H NMR spectrum of chitosan (DD = 78%) dissolved in D_2O/CD_3COOD. The chemical structure of a chitosan chain not-completely N-deacetylated is reported in the figure.

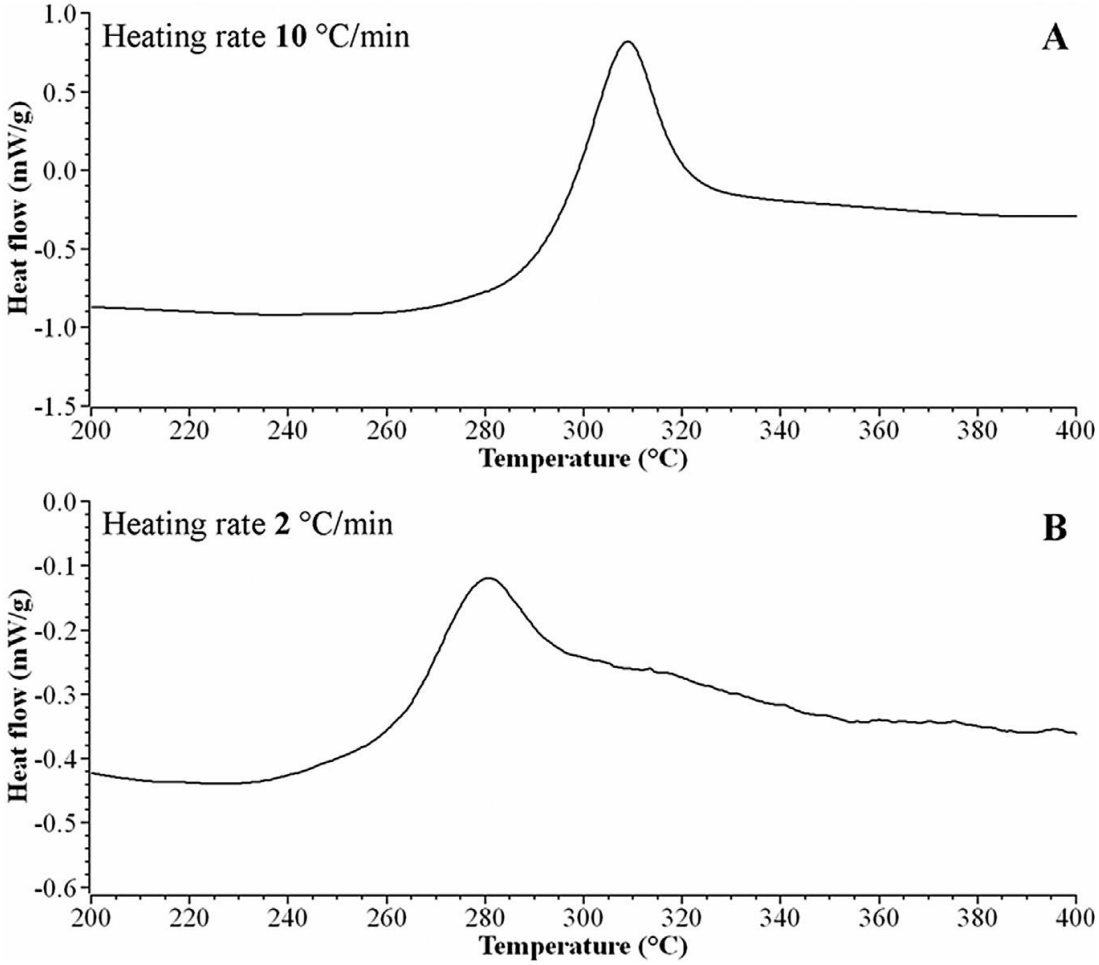

Fig. 3. DSC thermograms in the 200-400 °C range of chitosan (DD = 78%) powder heated under dynamic flow of nitrogen at different heating rates: 10 °C min^{-1} (A), 2 °C min^{-1} (B).

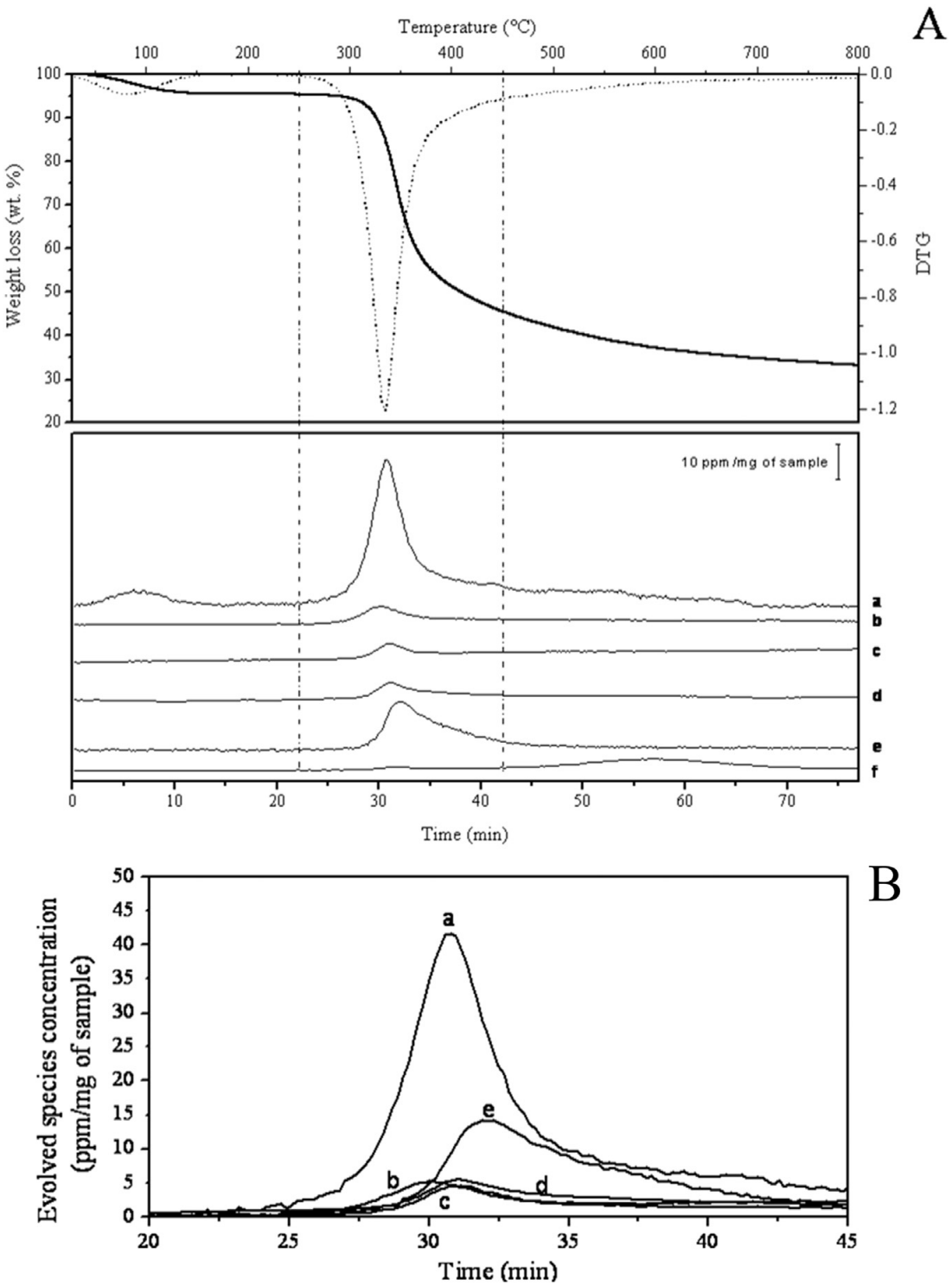

Fig. 4. (A) Upper panel: TGA (solid line) and the derivative (dotted line) curves of the chitosan (DD = 78%) heated from 30 to 800 °C at 10 °C min^{-1} under dynamic nitrogen atmosphere. Lower panel: FTIR profiles of the volatile products released from chitosan during the heating ramp expressed as a function of temperature/time. Each curve represents the concentration (ppm/mg of sample) of the species evolved and is obtained relating the IR absorbance at a specific wavenumber to the concentration by the Lambert-Beer's law relationship: H_2O (line a, 3566 cm^{-1}), NH_3 (line b, 965 cm^{-1}), CO (line c, 2185 cm^{-1}), CO_2 (line d, 2359 cm^{-1}), CH_3COOH (line e, 1179 cm^{-1}), and CH_4 (line f, 3016 cm^{-1}). (B): magnification of the FTIR profiles of the species evolved during the decomposition of chitosan under N_2: H_2O (line a), NH_3 (line b), CO (line c), CO_2 (line d), CH_3COOH (line e).

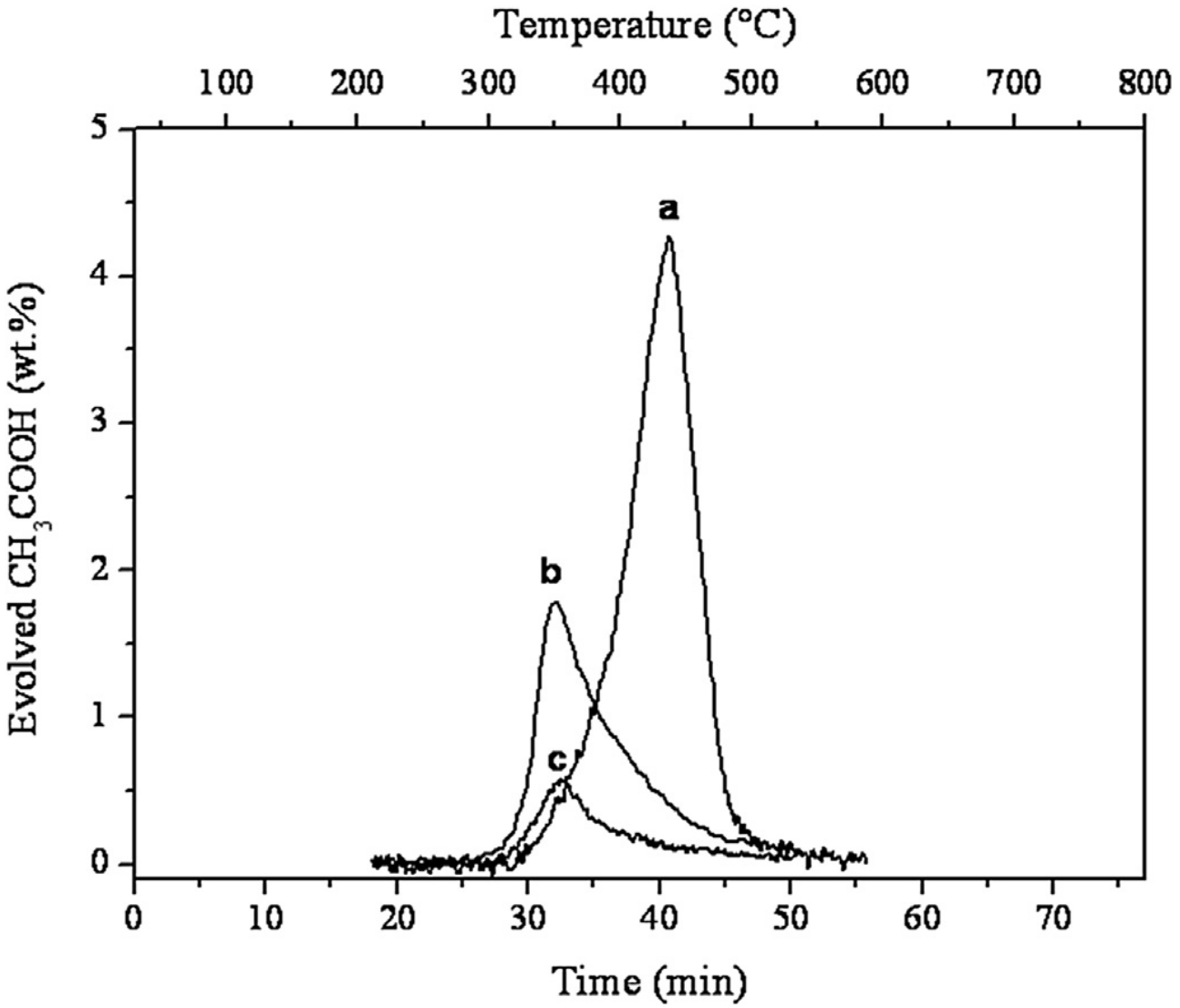

Fig. 5. Kinetic of acetic acid release (i.e. N-deacetylation) as a function of temperature/time measured as CH3COOH evolved from: chitin (a), chitosan (DD = 78%) (b), and medical grade chitosan (DD > 93%) (c). Refer to Fig. ESI-6 for further details.

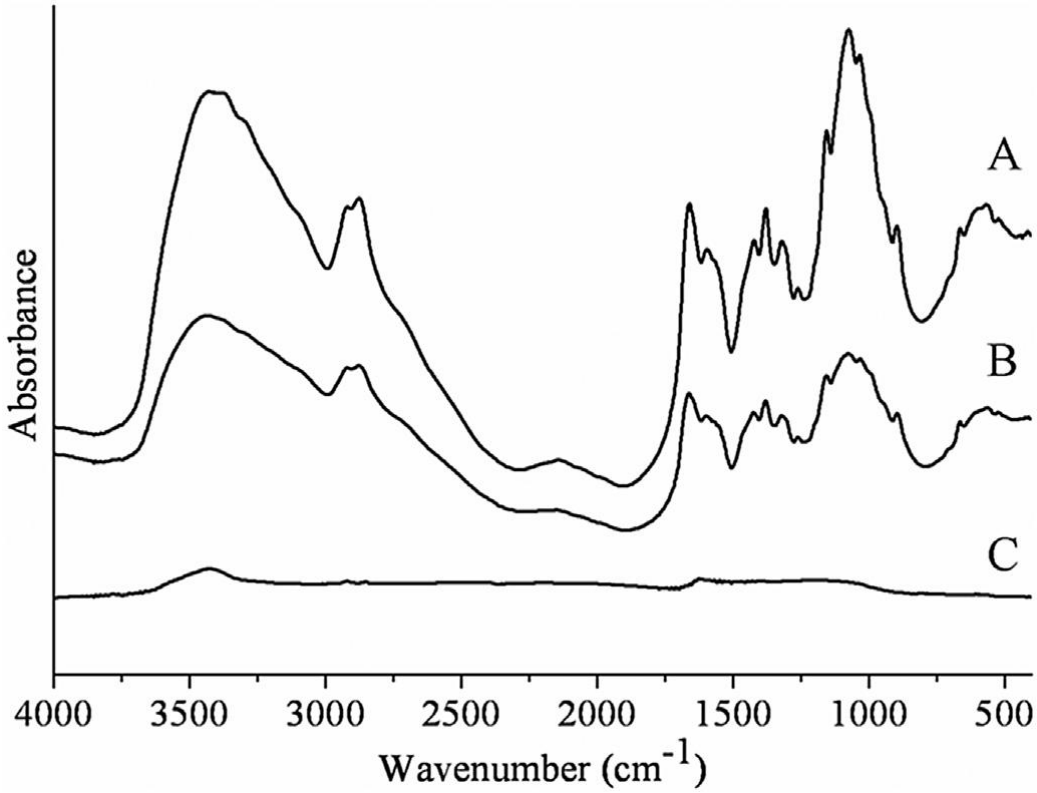

Fig. 6. Absorbance FTIR spectra of chitosan (DD = 78%) sample in the 4000-400 cm^{-1} range collected in transmission mode. Not-treated material (A), chitosan after drying at 200 °C (B) and after degradation at 800 °C (C). All the spectra were obtained by dispersing the powdery sample in KBr.

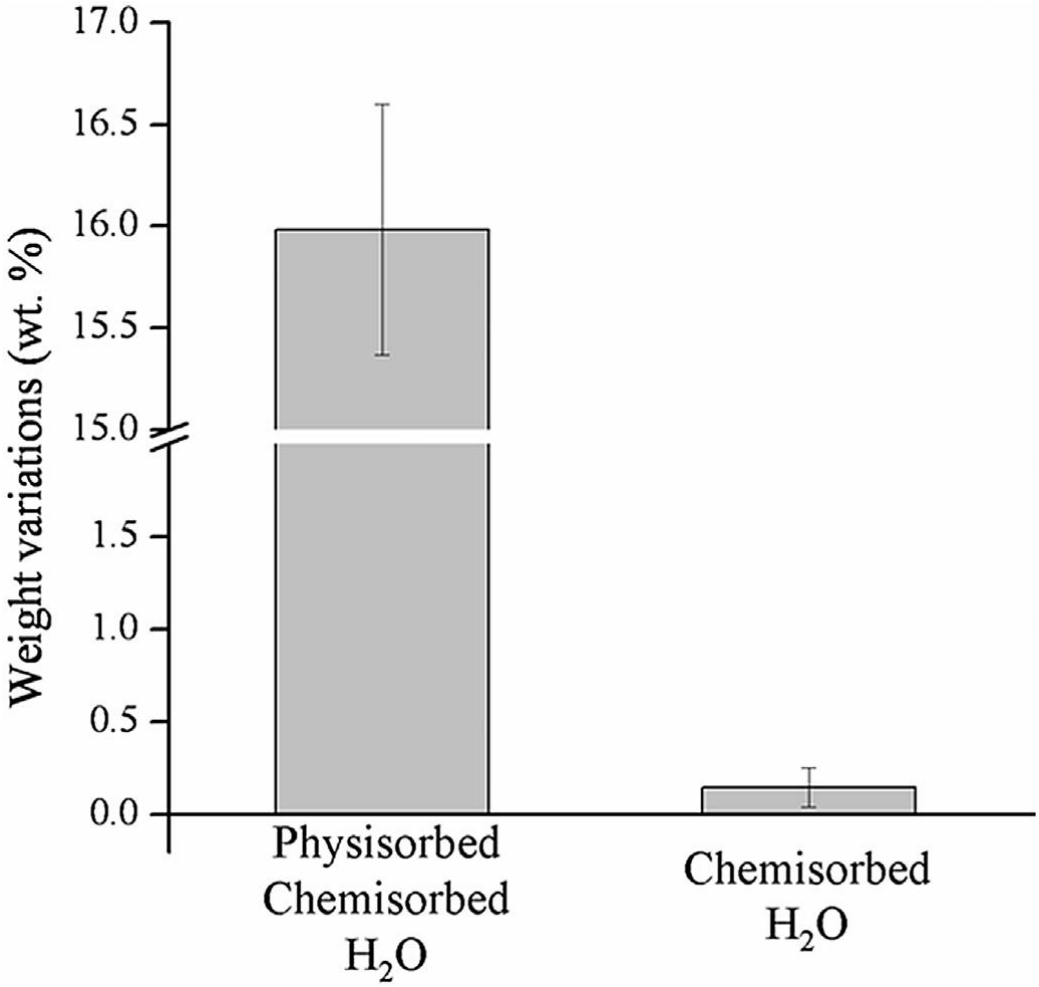

Fig. 7. Thermo-microgravimetric analyses on chitosan (DD = 78%) powder. Effect of 20 mbar water vapors adsorption/desorption upon three cycles after thermal treatment 3 °C/min-130-RT: wt.% increase induced by 20 mbar water adsorption (physisorbed and chemisorbed H_2O histogram) and wt.% reduction after outgassing at RT (chemisorbed H_2O histogram).

Table 1. H_2O, NH_3, CO, CO_2 and CH_3COOH contribution to the pyrolysis.

Samples	H_2O (wt.%)	NH_3 (wt.%)	CO (wt.%)	CO_2 (wt.%)	CH_3COOH (wt.%)
Chitin	43.0	0.00	5.50	2.40	28.7
Chitosan (DD = 78%)	30.3	3.85	3.60	2.75	13.8
Chitosan (DD > 93%)	37.7	3.95	2.00	2.70	4.30